American Mineralogist, Volume 90, pages 1900–1908, 2005

Single-crystal X-ray diffraction of spinels from the San Carlos Volcanic Field, Arizona: Spinel as a geothermometer

HINAKO UCHIDA,[1,*] BARBARA LAVINA,[2] ROBERT T. DOWNS,[1] AND JOHN CHESLEY[1]

[1] Department of Geosciences, University of Arizona, Tucson, Arizona 85721-0077, U.S.A.
[2] Dipartimento di Mineralogia e Petrologia, Università di Padova, Corso Garibaldi 37, 35137, Padova, Italy

ABSTRACT

Fourteen spinels from two types of mantle xenoliths from the San Carlos Volcanic Field in Arizona were characterized using single-crystal X-ray diffraction and electron microprobe analysis. The dominant feature seen in the chemistry of spinels from the Group I xenoliths is the extensive substitution of Cr for Al ($Cr_{0.20}Al_{1.76}$ to $Cr_{0.83}Al_{1.10}$) correlated with Mg for Fe^{2+} ($Mg_{0.69}Fe^{2+}_{0.31}$ to $Mg_{0.80}Fe^{2+}_{0.19}$). Although Group II spinels display consistently low Cr values, they also show a well-correlated substitution of Mg for Fe^{2+} ($Mg_{0.63}Fe^{2+}_{0.37}$ to $Mg_{0.69}Fe^{2+}_{0.31}$). Unit-cell parameters for spinels from the Group I xenoliths range from 8.1259 to 8.2167 Å, while those from the Group II xenoliths range from 8.1247 to 8.1569 Å. The cell parameters are linearly correlated with Fe^{2+} and Cr contents. Cation distributions were determined from experimental bond lengths and refined site occupancies using the algorithm of Lavina et al. (2002). The San Carlos spinels display variable degrees of order, with inversion parameters ranging from 0.10 to 0.16 for Group I and from 0.17 to 0.22 for Group II. Closure temperatures were computed with the Princivalle equation, giving averages of 808(37) °C for spinels from Group I xenoliths and 822(62) °C for samples from Group II xenoliths. We show that these results are reasonable, and thus extend the use of the Princivalle equation, or at least its functional form, to samples with significant Cr and Fe^{2+} contents. This study demonstrates that, in spite of the extensive chemical variability of the San Carlos spinels, and given that the origins of the two groups of xenoliths are different, the oxygen coordinates remain fixed, suggesting that the oxygen coordinate is a function of thermal history.

INTRODUCTION

Peridot Mesa in the San Carlos Indian Reservation, Arizona, is a late Tertiary to Quaternary basalt flow that contains abundant ultramafic xenoliths (Bromfield and Schride 1956). Bernatowicz (1981) obtained a K-Ar age of 0.58 ± 0.21 Ma for the Peridot Mesa Vent. The geology of the San Carlos Volcanic Field was described by Marlowe (1961) and Wohletz (1978). Spinel lherzolite, pyroxenite, and herzbergite xenoliths have all been reported from San Carlos (Galer and O'Nions 1989).

Mantle xenoliths are classified into two general types, defined primarily on the basis of major-element chemistry. In this paper they are designated as Group I and Group II, which corresponds to Group I and II of Frey and Prinz (1978) and to the Cr-diopside and Al-augite groups of Wilshire and Shervais (1975). Petrographic description of the San Carlos xenoliths can be found in Table 1 of Frey and Prinz (1978). Detailed geochemical and isotopic studies of San Carlos xenoliths have been reported by many authors (cf. Zartman and Tera 1973; Frey and Green 1974; Frey and Prinz 1978; Zindler and Jagoutz 1980, 1988; Galer and O'Nion 1989). The petrogenesis of mantle xenoliths has been the subject of much investigation. The REE studies of Frey and Prinz (1978) suggested that Group I xenoliths are not genetically related to the host basalt but rather represent a residue after extraction of various degrees of partial melt. In contrast, Group II xenoliths seem to be chemically related to the host lava and represent cumulate rocks produced by fractional crystallization of an evolved magma that was derived from the host magma earlier than the volcanic episodes.

Equilibration temperature and pressure of crystallization for peridotites can be estimated by a variety of thermometers using chemical exchange reactions between coexisting minerals. For example, Brey and Köhler (1990) estimated an equilibration temperature of 1052 °C for the San Carlos spinel lherzolite using two coexisting pyroxenes. Köhler and Brey (1990) estimated an equilibration pressure of 12.7 kbar for Group I spinel lherzolites with mg-number ~90 from San Carlos using Ca exchange between olivine and clinopyroxene.

The temperature and pressure conditions of mantle xenoliths can also be ascertained by examining the relative occupancies of elements between crystallographically distinct sites within a single mineral phase. The methodology for this is still in the developmental stage but important studies include Stimpfl et al. (1999) and Stimpfl (2003) who studied thermodynamics and kinetics of the Fe-Mg order-disorder process in orthopyroxene to determine the cooling rates of the crystals, and Nimis (1995, 1999) and Nimis and Ulmer (1998) who investigated variations in the crystal structural parameters of *C*2/*c* clinopyroxene in response to increasing pressure and concluded that chemical substitution at the two cation sites allows the cell volume to decrease without inducing lattice strain.

Another potential way to study the pressure-temperature history of mantle xenoliths would be to conduct a complete crystal-chemical study, including unit-cell parameters, crystal

* E-mail: uchida@geo.arizona.edu

0003-004X/05/1112–1900$05.00/DOI: 10.2138/am.2005.1795

structures, and site occupancies, of all the phases in a xenolith. In this way, one could combine both of the methods described above; examining not only the comparative chemistries of coexisting minerals, but also the comparative chemistries of individual crystallographic sites within a single phase.

We begin our study by describing the crystal chemical systematics observed in spinels from 13 distinct xenoliths, of both Group I and II, from San Carlos. In later papers, we will describe the crystal chemistry and intracrystalline-intercrystalline partitioning of major elements in all the minerals from the same xenolith samples, with the goal of establishing a correlation between the different phases and potentially a useful and precise description of petrological conditions and history.

The structures and site occupancies of natural and synthetic spinels have been studied using single-crystal X-ray diffraction techniques at both room and higher-temperature conditions (cf. Hill et al. 1979; Della Giusta et al. 1996; Lucchesi et al. 1998; Andreozzi et al. 2000; Carbonin et al. 2002; Andreozzi and Lucchesi 2002). The spinel structure can be described as a slightly distorted cubic close-packed array of 32 oxygen atoms with 8 cations at tetrahedral (T) sites, and 16 cations at octahedral (M) sites per unit cell (Hill et al. 1979). The T and M sites lie on special positions with $\bar{4}$3m and $\bar{3}$m symmetry, respectively. The only variable structural parameters are the unit-cell dimension (a) and oxygen coordinate (u,u,u), which is related to the oxygen packing distortion. The ideal ccp structure shows $u = 0.25$, and it is observed that $u > 0.25$ for the spinels found in mantle xenoliths. The observed distortion is a consequence of similar M-O and T-O bond distances ($u = 0.2625$ when distances are equal; Hill et al. 1979). The unit-cell parameter, a, primarily varies according to bulk chemical composition whereas u varies with cation distribution between the T and M sites since it is geometrically related to the ratio of the bond distances (Princivalle et al. 1989);

$$u = \frac{0.75R - 2 + \sqrt{(33/16)R - 0.5}}{6(R-1)}$$

where $R = (\text{M-O})^2/(\text{T-O})^2$ and T-O and M-O represent the bond distances. Hazen and Navrotsky (1996) showed that the unit-cell volume is dependent only on the tetrahedral and octahedral bond lengths, with the octahedral bonds exerting the greater influence. Princivalle et al. (1989) observed that u displays a constant value within the spinels from individual geological settings, even if there is a variation in bulk chemistry, whereas spinels with similar bulk chemistry but belonging to different geological environments exhibit a wide range of u values. This observation indicates that natural spinels at room condition may not be in equilibrium. Therefore, their crystallographic parameters must preserve geologic history. Thermal experiments employing spinels of fixed chemistry (cf. Della Giusta et al. 1996; Redfern et al. 1999) showed that the most sensitive parameter during changes in temperature is the oxygen coordinate, with u in normal spinels decreasing significantly during heating and increasing during cooling. Conflicting reports on the variation of u with pressure are in literature. Pavese et al. (1999) show that u decreases with increasing pressure while Levy et al. (2003) show that u and P are not correlated. Thompson and Downs (2001) demonstrated that there is a relationship between the distortion from closest packing and P and T.

The spinel structure can incorporate a variety of different cations at its tetrahedral and octahedral sites, resulting in a temperature-pressure stability field that is larger than for pure $MgAl_2O_4$. There are two end-member cation distributions in the spinels commonly referred to as normal, $X[Y_2]O_4$, and inverse, $Y[XY]O_4$, where X represents divalent cations, Y represents trivalent cations, and the brackets indicate the octahedral site. Most natural spinels are disordered and lie between these two end-members. The disordered configuration may be written as $^{IV}(X_{1-i}Y_i)^{VI}[X_iY_{2-i}]O_4$, where intracrystalline disorder is defined by the inversion parameter, i. Thus, $i = 0$ for an end-member normal spinel, and $i = 1$ for an end-member inverse spinel (Hill et al. 1979). A totally random arrangement is obtained when $i = 2/3$. There are extensive studies on temperature-dependent cation order-disorder using neutron and X-ray powder diffraction methods over a broad temperature range (cf. Peterson et al. 1991; O'Neill 1994; Redfern et al. 1999; O'Neill et al. 2003). In addition to dependency of cation distribution on temperature, the influence of bulk composition on such disorder is also a crucial factor (O'Neill and Navrotsky 1983; Lavina et al. 2003).

The intracrystalline ordering of a crystal is dependent on the cooling rate and kinetics of ordering. When the temperature decreases rapidly, the rate of ordering falls behind the cooling rate and the crystal is no longer in equilibrium with the temperature, where the kinetically controlled ordering path diverges from the equilibrium ordering path (Ganguly 1982). The quenching temperature (T_Q) is defined as the temperature at which the ordering reaction stops and the ordering state observed at room condition is effectively established. The closure temperature (T_c) is defined as the projected temperature of T_Q onto the equilibrium ordering path. The difference between T_Q and T_c is a function of cooling rate (Ganguly 1982). Several investigators have studied the relationships between intracrystalline disorder and closure temperature (Schmocker and Waldner 1976; Basso et al. 1984; Della Giusta et al. 1986; Princivalle et al. 1989; Lucchesi and Della Giusta 1997; and Lucchesi et al. 1998). Rapidly cooled crystals display a higher closure temperature than crystals that are cooled slowly, and consequently, rapidly cooled crystals display a higher degree of disorder.

EXPERIMENTAL METHODS

Fourteen spinel samples were selected from 13 xenoliths collected by the authors from Peridot Mesa, San Carlos Volcanic Field, Arizona. The specific location at Peridot Mesa corresponds to location no. 2 on Figure 2 of Galer and O'Nions (1989), an operating peridot gem mine run by T. and E. Goseyun. Two crystals (SC19 and SC19-2) from one of the xenoliths were analyzed to characterize consistency and establish an estimate of the systematic errors of our chemistry and structure refinements. The sizes of the xenoliths found at the site range from less than a centimeter to approximately half a meter in diameter. Spinel crystals chosen for this experiment were up to 1 mm in diameter, and examinations by electron microprobe did not indicate zoning. They were crushed to approximately 100 μm size and were selected for further study after examination of their diffraction profiles. Peak widths from ω-scans ranged from 0.085° to 0.100° and represent very well-crystallized samples. Descriptions of color, crystal size, and the type of xenolith from which each crystal was picked are found in Table 1. The spinels appear to be opaque and black in the rock specimens, but are translucent and show colors such as purple, brown, and black when they are approximately 10 μm thick or less.

Diffracted peak positions and intensities were measured with a Picker diffractometer using unfiltered Mo$K\alpha$ radiation at 45 kV and 40 mA that has been automated with a Windows-based Visual-Fortran code extensively modified after the SINGLE software written by L. Finger and described in Angel et al. (2000). All crystals were examined under the same set of conditions. The precise positions of 10 peaks between $17° < 2\theta < 26°$ were determined using a modification of the

8-position centering technique of King and Finger (1979) in which both $K\alpha1$ and $K\alpha2$ profiles are fit with Gaussian functions. The cell parameters for each crystal were refined from the measured positions of the same set of reflections and are reported in Table 2. Intensities were collected to $2\theta \leq 60°$ using ω scans of 1° width, a step size of 0.025°, and 5 s per step counting times. Examination of observed intensities indicated $Fd\bar{3}m$ symmetry, as expected. The structures were refined using F with anisotropic displacement parameters and chemical constraints using a modification of RFINE (Finger and Prince 1975) to *Rw* ranging from 0.003 (SC2) to 0.027 (SC19). Eight parameters were refined; the scale factor, secondary extinction coefficient (Ext), oxygen coordinate, and displacement parameters. To avoid the effects of strong correlations, the site occupancy values were not automatically refined, but were manually adjusted until we found the global minimum for *Rw*. The structure factors were weighted by $w = [\sigma_F^2 + (pF)^2]^{-1}$, where σ_F was obtained from counting statistics and *p* chosen to insure normally distributed errors (Ibers and Hamilton 1974). In particular, the constraint that the errors are normally distributed may produce a higher value of *Rw*, but it insures a uniformly comparable set of data for all the crystals (Hamilton 1974). We performed absorption correction on 6 samples by measuring the crystal shapes and using the program absorb95, modified after Burnham (1966). The correction did not produce any significant difference in the refinement. The refinement results are listed in Table 2. To test any dependency of the refined parameters on 2θ, we selected a crystal from one of our xenoliths (SC8) and recorded intensities for reflections to $2\theta = 110°$. A comparison of the refined structure with that of a subset with reflections to 60° did not show significant differences in the refined occupancies and oxygen parameters.

After the X-ray data collection, the same crystals were mounted on glass slides and polished for electron microprobe analysis. They were analyzed with the Cameca SX50 electron microprobe at the University of Arizona, using an acceleration voltage of 15 kV, a beam current of 20 nA, a beam diameter of 2 μm, and 20 s counting times. Natural and synthetic standards were used: Mg = diopside; Si = forsterite (Fo_{90}) (synthetic); Al = spinel; Cr = chromite (synthetic); Ti = rutile; Mn = rhodonite; Fe = ilmenite (synthetic); Zn = gahnite; Ni = Ni-doped diopside; V = vanadium. The data were corrected for fluorescence, absorption, and atomic number effects using the PAP correction method (Pouchou and Pichoir 1991). On average, ten points were analyzed from each sample. The results of the chemical analysis are reported in Table 3.

The X-ray scattering factors of Mg and Al are very similar, making it difficult to refine the Mg and Al site occupancies from X-ray experiments. Although it is possible to obtain reasonable estimates of these occupancies with careful procedures, such as long counting times and the constraint that errors are normally distributed (cf. Bertolo and Nimis 1993), it is likely that the Mg/Al site occupancies represent the most significant error in the refined cation distributions. In addition to the similar scattering of Al and Mg, the complex chemistries of the spinels from San Carlos also made the refinement of cation distributions problematic. Therefore we optimized the atomic fractions at each site (X_i) using the SIDR minimization routine reported by Lavina et al. (2002). The procedure is essentially based on two assumptions: (1) that the bond lengths are a linear combination of site atomic fractions multiplied by their characteristic bond distances in spinel (except for Fe^{3+} and Ni^{2+}, which require additional corrections; Lavina et al. 2002) and (2) that the mean atomic number, man, is a linear function of site atomic fractions multiplied by associated atomic numbers. In the SIDR procedure, crystal chemical parameters are calculated as a function of variable site atomic fractions and are forced to match observed parameters through minimization of the following equation, $F(X_i)$,

$$F(X_i) = \frac{1}{n}\sum_j \left[\frac{O_j - C_j(X_i)}{\sigma_j}\right]^2$$

where O_j are nine observed quantities and three crystal chemical constraints, and σ_j are their standard deviations. In the case of the San Carlos spinels, the nine observed parameters are cell parameter, oxygen coordinate, mean atomic numbers calculated from the site occupancies of the refinement (man_T and man_M), and atoms per formula unit for the five major elements (Mg, Al, Fe^{2+}, Fe^{3+}, Cr). The standard deviations of *a* and *u* are reported in Table 2, and we fixed the standard deviation of atomic proportions to 2% for all elements because the experimentally determined standard deviations are very small and would rigidly constrain the optimization and weigh too heavily relative to other parameters. C_j were computed from the equations of Lavina et al. (2002) as a function of optimized variable cation fractions: Mg, Al, Fe^{2+}, and Fe^{3+} at the T site and Mg, Al, Fe^{2+}, Fe^{3+}, and Cr at the M site. For our samples, Cr, Ti, Ni, and V were constrained to the M site, whereas Si, Zn, and Mn were constrained to T. The three crystal-chemical quantities that contribute to the minimization function are the total site occupancies for the T (=1) and M (=2) sites and the sum of cation formal valence (= 8) with a σ value of 0.0005. The minimization led to a satisfactory agreement between observed and calculated parameters with $F(X_i)$ ranging from 0.1 to 1.1. The optimized cation distributions are listed in Table 4. The differences between calculated and observed values in *a* and *u* are less than 1σ, and the differences in man_T and man_M are 0.0–0.4, as reported in the table. Although the behavior of the minimization function is different with respect to each of the X_i, we can roughly estimate uncertainties from 0.01 to 0.02 for the optimized atomic fractions. Uncertainties in the inversion parameter are considered not to exceed 0.02 apfu.

TABLE 1. San Carlos spinels: sample name, size, color, and corresponding xenolith type

Sample	Approximate crystal size (μm)	Color	Xenolith type
SC 16	103 × 84 × 90	Brownish black	Group I
SC Gem	65 × 129 × 58	Purple	Group I
SC 3	97 × 65 × 65	Reddish purple	Group I
SC 5	100 × 100 × 119	Purplish black	Group I
SC 15	97 × 97 × 97	Brownish black	Group I
SC 10	97 × 103 × 97	Reddish purple	Group I
SC 8	129 × 129 × 65	Brown	Group I
SC 2	129 × 129 × 109	Reddish brown	Group I
SC 19	116 × 148 × 142	Black	Group II
SC 19-2	90 × 45 × 52	Black	Group II
SC 1	180 × 142 × 123	Black	Group II
SC 11	84 × 129 × 129	Black	Group II
SC 20	129 × 148 × 110	Black	Group II
SC 14	97 × 129 × 161	Black	Group II

RESULTS AND DISCUSSION

Chemistry

The chemistries of the spinels from San Carlos lie in the field defined by the spinel ($MgAl_2O_4$)-hercynite ($FeAl_2O_4$)-magnesiochromite ($MgCr_2O_4$)-chromite ($FeCr_2O_4$) solid solution with minor Fe^{3+}. The dominant feature in the chemistry of spinels from Group I xenoliths is the extensive substitution along the spinel-magnesiochromite solid solution ($Cr_{0.20}Al_{1.76}$ to $Cr_{0.82}Al_{1.07}$), and to a lesser extent along the spinel-hercynite solid solution ($Mg_{0.72}Fe^{2+}_{0.27}$ to $Mg_{0.80}Fe^{2+}_{0.19}$). The Group II spinels display consistently low Cr values, but they are rich in hercynite component ($Mg_{0.63}Fe^{2+}_{0.36}$ to $Mg_{0.69}Fe^{2+}_{0.31}$). In Figure 1a, a clear relationship can be observed between Al and Cr content, however the relational trend is displaced from the line representing ideal substitution of end-member components. The deviation of the observed data from this line is a measure of the presence of other trivalent cations, mainly Fe^{3+}. A relationship between Mg and Fe^{2+} content is also observed (Fig. 1b), and Fe and Mg fall closely along the line of ideal substitution because the amounts of other divalent cations are always small and rather constant. The major elemental composition of our samples is shown in Figure 1c, where $Cr/(Cr + Al + Fe^{3+})$ is plotted against $Mg/(Mg + Fe^{2+})$. This plot shows a distinct separation between Group I and II xenoliths, with Group I richer in Mg and Cr. Spinels from Group I xenoliths show a broad compositional range and increasing Cr content is roughly correlated with increasing Fe^{2+}. In Group II, there are four samples with low Cr contents (below 0.08 apfu) and two samples with higher Cr contents (0.23 apfu). Those samples with lower Cr contents correspond to the previously reported compositional range for Group II (Frey and Prinz 1978) and are indicated with triangles. This distinct separation in chemistry between the two groups is also well explained by the petrological model proposed by Frey and Prinz (1978), Group I xenoliths representing residue and Group II being cumulates

TABLE 2. Structural refinement results

Sample	SC 16	SC Gem	SC 3	SC 5	SC 15
a (Å)	8.2112(1)	8.2167(2)	8.1866(1)	8.20334(9)	8.1831(2)
V (Å^3)	553.64(3)	554.74(3)	548.68(3)	552.04(2)	547.96(3)
R_{merge}	0.020	0.016	0.023	0.021	0.010
R_w	0.014	0.017	0.010	0.015	0.016
p	0.01229	0.01508	0.00827	0.01532	0.01590
T-β_{11}	0.00246(10)	0.00222(11)	0.00249(8)	0.00220(11)	0.00242(10)
M-β_{11}	0.00184(9)	0.00190(10)	0.00175(7)	0.00176(10)	0.00241(10)
M-β_{12}	–0.00010(3)	–0.00006(3)	–0.00009(2)	–0.00008(3)	–0.00010(3)
u	0.26274(11)	0.26270(14)	0.26288(9)	0.26284(14)	0.26279(12)
O-β_{11}	0.00256(12)	0.00251(14)	0.00254(9)	0.00250(13)	0.00298(12)
O-β_{12}	–0.00016(7)	–0.00013(8)	–0.00013(6)	–0.00017(7)	–0.00015(6)
T-O (Å)	1.9589(5)	1.9597(7)	1.9552(4)	1.9585(7)	1.9530(6)
M-O (Å)	1.9538(9)	1.9554(12)	1.9469(8)	1.9512(11)	1.9467(10)
Polyhedral volume T (Å^3)	3.8581	3.8624	3.8352	3.8554	3.8227
Polyhedral volume M (Å^3)	9.7768	9.8019	9.6701	9.7351	9.6700
man T	15.91	15.63	15.78	16.62	15.85
man M	17.95	18.215	16.84	17.23	16.58

Sample	SC 10	SC 8	SC 2	SC 19	SC 19-2
a (Å)	8.1544(1)	8.1520(2)	8.1259(1)	8.1569(2)	8.1566(2)
V (Å^3)	542.22(3)	541.74(3)	536.55(3)	542.71(4)	542.67(4)
R_{merge}	0.010	0.014	0.013	0.026	0.014
R_w	0.015	0.021	0.003	0.027	0.023
p	0.01316	0.02070	0.001939	0.02668	0.02071
T-β_{11}	0.00232(10)	0.00192(13)	0.00208(4)	0.00214(17)	0.00320(15)
M-β_{11}	0.00178(9)	0.00191(12)	0.00201(4)	0.00198(16)	0.00233(14)
M-β_{12}	–0.00007(3)	–0.00007(3)	–0.00008(2)	–0.00013(4)	–0.00010(5)
u	0.26315(11)	0.26287(14)	0.26293(7)	0.26302(17)	0.26295(15)
O-β_{11}	0.00234(11)	0.00259(14)	0.00268(4)	0.00286(17)	0.00347(17)
O-β_{12}	–0.00004(6)	–.00003(7)	–0.00006(3)	–0.00011(8)	0.00006(11)
T-O (Å)	1.9511(5)	1.9466(7)	1.9414(2)	1.9499(8)	1.9488(7)
M-O (Å)	1.9374(9)	1.9388(12)	1.9321(3)	1.9389(14)	1.9393(12)
Polyhedral volume T (Å^3)	3.8124	3.7859	3.7554	3.8051	3.7989
Polyhedral volume M (Å^3)	9.5203	9.5494	9.4487	9.5465	9.5548
man T	15.27	15.13	14.58	17.11	17.58
man M	15.68	15.44	14.48	15.16	14.80

Sample	SC 1	SC 11	SC 20	SC 14
a (Å)	8.1357(2)	8.1291(1)	8.1356(2)	8.1247(2)
V (Å^3)	538.50(4)	537.19(3)	538.51(3)	536.32(4)
R_{merge}	0.013	0.028	0.019	0.013
R_w	0.020	0.024	0.021	0.012
p	0.02080	0.02773	0.02306	0.01553
T-β_{11}	0.00241(15)	0.00241(15)	0.00204(15)	0.00233(10)
M-β_{11}	0.00162(15)	0.00256(14)	0.00204(14)	0.00231(9)
M-β_{12}	–0.00004(5)	–0.00017(4)	–0.00013(3)	–0.00009(2)
u	0.26302(15)	0.26273(15)	0.26286(13)	0.26280(9)
O-β_{11}	0.00268(19)	0.00335(16)	0.00288(15)	0.00309(10)
O-β_{12}	0.00005(8)	0.00004(8)	0.00000(7)	0.00002(5)
T-O (Å)	1.9449(7)	1.9393(7)	1.9427(6)	1.9392(4)
M-O (Å)	1.9338(12)	1.9343(12)	1.9349(11)	1.9328(7)
Polyhedral volume T (Å^3)	3.7755	3.7427	3.7623	3.7423
Polyhedral volume M (Å^3)	9.4723	9.4877	9.4932	9.4631
man T	17.67	16.35	16.86	16.26
man M	13.96	14.15	14.24	13.90

Notes: Space group: $Fd\bar{3}m$.
Tetrahedral site, T, located at [1/8, 1/8, 1/8], $\beta_{11} = \beta_{22} = \beta_{33}$, $\beta_{12} = \beta_{13} = \beta_{23} \equiv 0$.
Octahedral site, M, located at [1/2, 1/2, 1/2], $\beta_{11} = \beta_{22} = \beta_{33}$, $\beta_{12} = \beta_{13} = \beta_{23}$.
O located at [*u*, *u*, *u*], $\beta_{11} = \beta_{22} = \beta_{33}$, $\beta_{12} = \beta_{13} = \beta_{23}$.

from more evolved magma. In summary, the chemistry of the spinels in this study, with the exception of spinels with high Cr contents from a Group II xenolith, spans the same compositional range as previously reported (Galer and O'Nions 1989; Frey and Prinz 1978), as indicated by solid triangles and open triangles, respectively, in these three figures. In addition to these major elements, our samples also contain Fe^{3+} ranging from 0.02 to 0.14 apfu and minor amounts of Ti, Zn, Mn, V, and Ni.

Crystal chemistry

The unit-cell parameters and cell volumes for spinels from the Group I xenoliths range from 8.1259–8.2167 Å and from 536.55–554.74 Å^3, respectively, while for Group II xenoliths they range from 8.1247–8.1569 Å and 536.32–542.71 Å^3, respectively. Cell parameters of the spinels from the Group II xenoliths, in general, are smaller than those from the Group I xenoliths although there are some Group I spinels that are just as small. The observed cell parameters were plotted against Fe^{2+} and Cr contents, respectively, and the variations in cell parameters can be positively correlated to Fe^{2+} and Cr contents (Figs. 2a and 2b). This is simply a consequence of the shorter Mg-O and Al-O bond distances relative to those for Fe^{2+}-O and Cr-O. These figures show two distinct populations defined by Group I and II xenoliths. Data within each distinct population show

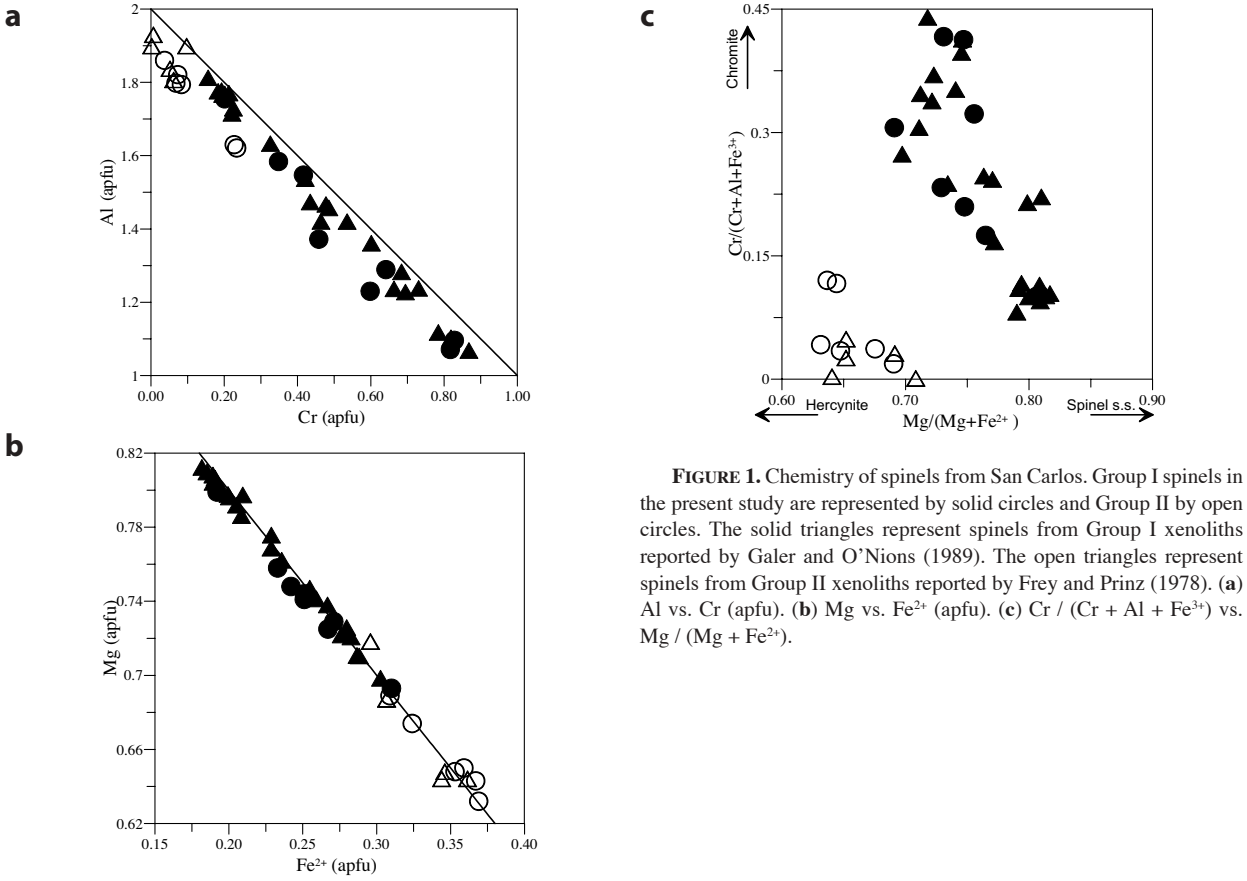

FIGURE 1. Chemistry of spinels from San Carlos. Group I spinels in the present study are represented by solid circles and Group II by open circles. The solid triangles represent spinels from Group I xenoliths reported by Galer and O'Nions (1989). The open triangles represent spinels from Group II xenoliths reported by Frey and Prinz (1978). (**a**) Al vs. Cr (apfu). (**b**) Mg vs. Fe^{2+} (apfu). (**c**) Cr / (Cr + Al + Fe^{3+}) vs. Mg / (Mg + Fe^{2+}).

TABLE 3. San Carlos spinels: results of microprobe analysis

	SC 16	SC Gem	SC 3	SC 5	SC 15	SC 10	SC 8	SC 2	SC 19	SC 19-2	SC 1	SC 11	SC 20	SC 14
MgO	16.81	17.01	17.67	16.21	17.56	18.33	18.90	20.71	15.75	15.95	15.74	17.11	16.42	17.65
Al_2O_3	32.12	31.09	38.48	36.38	41.80	48.21	49.92	57.52	50.20	50.53	56.55	58.44	57.58	60.26
Cr_2O_3	36.20	35.34	28.54	26.38	20.81	19.32	16.34	9.81	10.82	10.50	3.88	3.49	3.22	1.77
SiO_2	0.06	0.07	0.04	0.06	0.10	0.07	0.04†	0.04	0.10	0.09	0.11	0.05†	0.07	0.05†
TiO_2	0.14	0.30	0.18	0.85	0.58	0.22	0.16	0.13	1.04	0.98	0.44	0.47	0.55	0.38
MnO	0.26	0.31	0.24	0.24	0.23	0.17	0.19	0.13	0.21	0.20	0.15	0.16	0.15	0.14
FeO	13.66	14.02	12.56	18.25	17.44	11.98	12.92	10.50	20.05	19.75	20.84	18.35	20.73	17.85
ZnO	0.11	0.09†	0.13†	0.14†	0.17	0.03†	0.11†	0.08†	0.12†	0.15†	0.18†	0.16	0.09	0.13†
NiO	0.18	0.28	0.25	0.34	0.28	0.32	0.33	0.40	0.29	0.27	0.20	0.27	0.27	0.26
V_2O_3	0.16	0.16	0.13	0.23	0.23	0.13	0.10†	0.08†	0.17	0.17		0.14	0.12	0.14
Total	99.70	98.68	98.25	99.09	99.19	98.78	99.02	99.40	98.76	98.61	98.10	98.66	99.22	98.65
FeO*	11.03	10.28	10.18	12.95	11.63	11.04	10.35	8.85	16.02	15.67	16.39	14.67	15.94	14.10
Fe_2O_3*	2.92	4.15	2.65	5.89	6.45	1.04	2.86	1.83	4.48	4.53	4.95	4.09	5.32	4.17
Cations on basis of 4 oxygen atoms														
Mg	0.725(12)	0.741(4)	0.748(13)	0.693(9)	0.729(1)	0.744(5)	0.758(3)	0.799(5)	0.643(5)	0.650(3)	0.632(9)	0.674(5)	0.648(3)	0.689(8)
Al	1.096(8)	1.071(7)	1.289(14)	1.230(6)	1.372(6)	1.547(4)	1.584(5)	1.755(4)	1.621(4)	1.630(5)	1.794(9)	1.821(6)	1.798(6)	1.860(4)
Cr	0.828(2)	0.817(4)	0.641(4)	0.598(4)	0.458(4)	0.416(4)	0.348(2)	0.201(3)	0.234(3)	0.227(2)	0.083(3)	0.073(1)	0.068(2)	0.037(1)
Si	0.002(1)	0.002(1)	0.001(1)	0.002(1)	0.003(1)	0.002(1)	0.001(1)	0.001(1)	0.003(1)	0.003(1)	0.003(1)	0.001(1)	0.002(1)	0.001(2)
Ti	0.003(1)	0.007(1)	0.004(1)	0.018(1)	0.012(1)	0.005(1)	0.003(2)	0.003(1)	0.022(1)	0.020(1)	0.009(1)	0.009(1)	0.011(1)	0.008(1)
Mn	0.006(1)	0.008(1)	0.006(1)	0.006(1)	0.005(1)	0.004(1)	0.004(1)	0.003(1)	0.005(1)	0.005(1)	0.004(1)	0.004(1)	0.004(1)	0.003(1)
Fe	0.331(9)	0.343(1)	0.299(3)	0.438(5)	0.406(6)	0.273(6)	0.291(3)	0.227(2)	0.459(5)	0.452(6)	0.469(3)	0.406(4)	0.459(3)	0.391(6)
Zn	0.002(1)	0.002(2)	0.003(1)	0.003(1)	0.003(1)	0.001(1)	0.002(1)	0.002(1)	0.002(2)	0.003(1)	0.004(1)	0.003(1)	0.002(2)	0.003(1)
Ni	0.004(1)	0.007(1)	0.006(1)	0.008(1)	0.006(1)	0.007(1)	0.007(1)	0.008(1)	0.006(1)	0.006(1)	0.004(1)	0.006(1)	0.006(1)	0.006(1)
V	0.004(1)	0.004(1)	0.003(1)	0.005(1)	0.005(1)	0.003(1)	0.002(1)	0.002(1)	0.004(1)	0.004(1)	–	0.003(1)	0.003(1)	0.003(1)
Fe^{2+}	0.267(12)	0.251(5)	0.242(13)	0.310(7)	0.271(1)	0.251(6)	0.233(4)	0.192(5)	0.367(4)	0.359(3)	0.369(8)	0.324(4)	0.353(3)	0.309(10)
Fe^{3+}	0.064(7)	0.091(6)	0.057(14)	0.127(5)	0.135(4)	0.021(1)	0.058(4)	0.036(5)	0.092(6)	0.093(6)	0.100(6)	0.081(4)	0.106(6)	0.082(6)

Notes: FeO and Fe_2O_3 were calculated according to Carmichael (1967). Values in parentheses are 1σ uncertainties.
* Calculated.
† Some of the analyzed spots are below the detection limit.

TABLE 4. Cation distribution, inversion parameter, and closure temperature (T_c)

Sample	SC 16	SC Gem	SC 3	SC 5	SC 15
Occ T	$Mg_{.651}Fe^{2+}_{.243}Fe^{3+}_{.029}$ $Al_{.067}Mn_{.006}$ $Si_{.002}Zn_{.002}$	$Mg_{.660}Fe^{2+}_{.222}Fe^{3+}_{.045}$ $Al_{.062}Mn_{.008}$ $Si_{.002}Zn_{.002}$	$Mg_{.627}Fe^{2+}_{.236}Fe^{3+}_{.034}$ $Al_{.094}Mn_{.006}$ $Si_{.001}Zn_{.003}$	$Mg_{.591}Fe^{2+}_{.262}Fe^{3+}_{.069}$ $Al_{.068}Mn_{.006}$ $Si_{.002}Zn_{.003}$	$Mg_{.636}Fe^{2+}_{.218}Fe^{3+}_{.043}$ $Al_{.091}Mn_{.005}$ $Si_{.003}Zn_{.003}$
Occ M	$Al_{.517}Fe^{2+}_{.011}Fe^{3+}_{.017}$ $Cr_{.413}Mg_{.035}$ $V_{.002}Ni_{.002}Ti_{.002}$	$Al_{.517}Fe^{2+}_{.014}Fe^{3+}_{.023}$ $Cr_{.397}Mg_{.041}$ $V_{.002}Ni_{.003}Ti_{.003}$	$Al_{.608}Fe^{2+}_{.001}Fe^{3+}_{.011}$ $Cr_{.311}Mg_{.063}$ $V_{.002}Ni_{.003}Ti_{.002}$	$Al_{.588}Fe^{2+}_{.022}Fe^{3+}_{.029}$ $Cr_{.292}Mg_{.053}$ $V_{.003}Ni_{.004}Ti_{.009}$	$Al_{.653}Fe^{2+}_{.023}Fe^{3+}_{.045}$ $Cr_{.219}Mg_{.049}$ $V_{.003}Ni_{.003}Ti_{.006}$
F(*Xi*)	0.24	0.91	0.91	0.72	1.12
Δman_T (calc-obs)	0.1	0.3	0.2	0.2	0.0
Δman_M (calc-obs)	0.0	–0.3	–0.3	–0.2	–0.2
i	0.095	0.108	0.127	0.143	0.139
T_c (°C)	837	802	842	786	776
Sample	SC 10	SC 8	SC 2	SC 19	SC 19-2
Occ T	$Mg_{.638}Fe^{2+}_{.233}Fe^{3+}_{.009}$ $Al_{.113}Mn_{.004}$ $Si_{.002}Zn_{.001}$	$Mg_{.632}Fe^{2+}_{.214}Fe^{3+}_{.003}$ $Al_{.144}Mn_{.004}$ $Si_{.001}Zn_{.002}$	$Mg_{.656}Fe^{2+}_{.173}Fe^{3+}_{.013}$ $Al_{.152}Mn_{.003}$ $Si_{.001}Zn_{.002}$	$Mg_{.507}Fe^{2+}_{.321}Fe^{3+}_{.029}$ $Al_{.132}Mn_{.005}$ $Si_{.003}Zn_{.002}$	$Mg_{.502}Fe^{2+}_{.299}Fe^{3+}_{.067}$ $Al_{.122}Mn_{.005}$ $Si_{.003}Zn_{.003}$
Occ M	$Al_{.718}Fe^{2+}_{.009}Fe^{3+}_{.006}$ $Cr_{.208}Mg_{.051}$ $V_{.001}Ni_{.004}Ti_{.002}$	$Al_{.721}Fe^{2+}_{.009}Fe^{3+}_{.028}$ $Cr_{.174}Mg_{.062}$ $V_{.001}Ni_{.004}Ti_{.002}$	$Al_{.803}Fe^{2+}_{.009}Fe^{3+}_{.011}$ $Cr_{.100}Mg_{.069}$ $V_{.001}Ni_{.004}Ti_{.001}$	$Al_{.746}Fe^{2+}_{.022}Fe^{3+}_{.032}$ $Cr_{.117}Mg_{.068}$ $V_{.002}Ni_{.003}Ti_{.011}$	$Al_{.754}Fe^{2+}_{.030}Fe^{3+}_{.014}$ $Cr_{.114}Mg_{.074}$ $V_{.002}Ni_{.003}Ti_{.010}$
F(*Xi*)	0.39	0.12	0.26	0.10	0.16
Δman_T (calc-obs)	0.3	0.1	0.2	0.0	–0.1
Δman_M (calc-obs)	–0.2	0.0	–0.1	–0.1	0.1
i	0.121	0.144	0.161	0.170	0.198
T_c (°C)	776	870	772	885	844
Sample	SC 1	SC 11	SC 20	SC 14	
Occ T	$Mg_{.498}Fe^{2+}_{.296}Fe^{3+}_{.081}$ $Al_{.114}Mn_{.004}$ $Si_{.003}Zn_{.004}$	$Mg_{.540}Fe^{2+}_{.238}Fe^{3+}_{.045}$ $Al_{.169}Mn_{.004}$ $Si_{.001}Zn_{.003}$	$Mg_{.534}Fe^{2+}_{.276}Fe^{3+}_{.028}$ $Al_{.155}Mn_{.004}$ $Si_{.002}Zn_{.002}$	$Mg_{.566}Fe^{2+}_{.217}Fe^{3+}_{.065}$ $Al_{.146}Mn_{.003}$ $Si_{.001}Zn_{.003}$	
Occ M	$Al_{.840}Fe^{2+}_{.036}Fe^{3+}_{.010}$ $Cr_{.041}Mg_{.066}$ $Ni_{.002}Ti_{.004}$	$Al_{.827}Fe^{2+}_{.042}Fe^{3+}_{.018}$ $Cr_{.036}Mg_{.067}$ $V_{.001}Ni_{.003}Ti_{.005}$	$Al_{.823}Fe^{2+}_{.039}Fe^{3+}_{.039}$ $Cr_{.034}Mg_{.056}$ $V_{.001}Ni_{.003}Ti_{.005}$	$Al_{.858}Fe^{2+}_{.045}Fe^{3+}_{.009}$ $Cr_{.018}Mg_{.062}$ $V_{.001}Ni_{.003}Ti_{.004}$	
F(*Xi*)	0.11	0.18	0.44	0.04	
Δman_T (calc-obs)	–0.2	–0.1	–0.4	–0.1	
Δman_M (calc-obs)	0.1	–0.3	0.2	0.0	
i	0.200	0.215	0.186	0.212	
T_c (°C)	734	867	845	757	

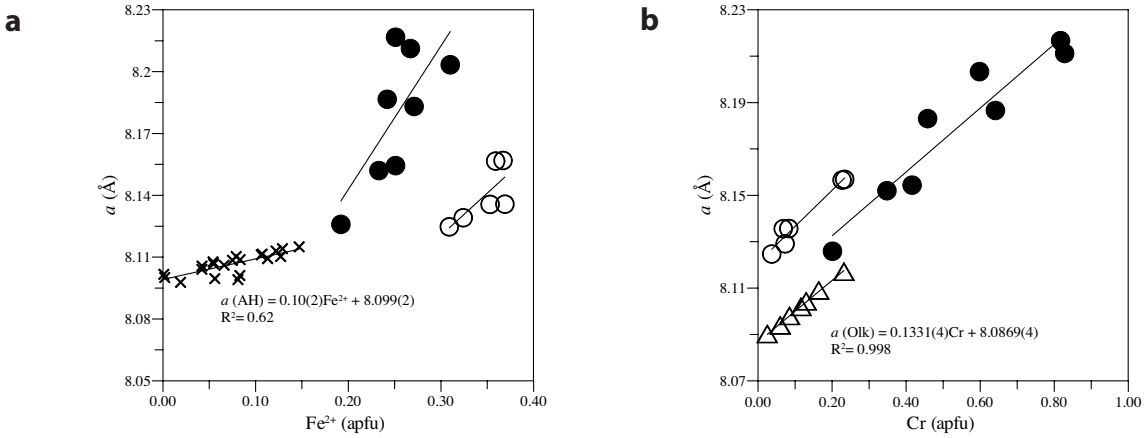

FIGURE 2. Unit-cell parameters plotted against (**a**) Fe^{2+} and (**b**) Cr contents. The solid and open circles represent spinels from Group I and II, respectively. The X's represent spinels from the Alban Hills (AH) volcanic region (Lucchesi et al. 1998). (**b**) The open triangles represent spinels from the Olkhon (Olk) metamorphic complex (Lavina et al. 2003).

a roughly linear variation, each with their own slope. Spinels from Group I xenoliths are dominated by a larger spread of cell parameters related to the large variation of Cr content, which influences the M-O bond distances significantly. The change in cell parameters in the spinels from Group II is relatively small, but increases linearly with the Fe^{2+} and Cr contents. By comparison, the spinels from the Alban Hills volcanic region (Lucchesi et al. 1998), which have Cr contents to 0.0009 apfu (Fig. 2a) are also plotted, and can be used as a reference for the Mg-Al-Fe^{2+} system. In Figure 2b we also include data for spinels from the Olkhon metamorphic complex that contain no Fe^{2+} (Lavina et al. 2003). In each figure, Group I and II have the same intercept,

8.00 (Fig. 2a) and 8.11 Å (Fig. 2b), but differ from the reference, 8.10 (AH) and 8.09 Å (Olk), respectively. The low Cr-containing samples from the Group II xenoliths are on the same linear trend as the samples from the Alban Hills (Fig. 2a). The high Cr content is responsible for the larger slope in both Group I and II with respect to the reference in this figure. Samples from both xenolith types display slopes that are similar to spinels from the Olkhon Metamorphic Complex, as shown in Figure 2b. The relationship between cell parameter and Fe^{2+}/Cr contents (apfu) in our samples is described by the following equation:

$$a = 8.085(15) + 0.136(13)*\mathrm{Cr} + 0.112(46)*\mathrm{Fe}^{2+},\ R^2 = 98.8\%.$$

The intercept value in this equation corresponds closely to the cell parameter of the spinel end-member, 8.0844(1) Å (Andreozzi et al. 2000).

Cation distribution and closure temperature

Inversion parameters for all the spinels were computed and are listed in Table 4. We calculated *i* using the definition of the inversion parameter, $^{IV}(X_{1-i}Y_i)^{VI}[X_iY_{2-i}]O_4$. For the spinels with complex chemistry, the inversion parameter is not only a function of temperature but also bulk composition. Therefore, it is important to understand whether the observed difference in *i* is due to different thermal history or different bulk composition. The inversion parameters of spinels from Group I range from 0.10 to 0.16, while those of spinels from Group II vary from 0.17 to 0.22. A linear relationship between *i* and Cr (Fig. 3) suggests that the differences found in *i* in our samples may be related to the effect of compositional changes rather than to different thermal histories.

Closure temperatures, T_c, for our samples were calculated using the equation from Princivalle et al. (1999):

$$T_c\ (°C) = 6640*B,$$

where $B = Al_T/(Al_T + Al_M) + 0.101(1 - Mg_T - Al_T) + 0.041(2 - Al_M - Mg_M)$. The calculated T_c for our samples are reported in Table 4. The average T_c for spinels from Group I and II xenoliths are 808(37) and 822(62) °C, respectively. We conclude that the closure temperatures for the two groups are the same within their standard deviations (Table 4). This conclusion agrees with our observation that the two types of xenoliths in this study exist together in the basalt lava flows in the limited area of topographic depression, and therefore they are expected to have similar cooling histories. The calculated closure temperatures for our samples as well as other localities are plotted as a function of Cr in Figure 4. The invariance of T_c with respect to Cr in this figure demonstrates that the equation of Princivalle et al. (1989) does not need additional terms to account for the effect of Cr.

As observed by Princivalle et al. (1989), spinels that underwent the same cooling history show rather constant *u* values in spite of their wide compositional ranges. In the San Carlos suites, oxygen coordinates for our samples range from 0.2627 (SCGem) to 0.2632 (SC10) for the spinels from Group I, and from 0.2627 (SC11) to 0.2630 (SC1 and SC19) for those from Group II. Since the oxygen coordinate, *u*, is a simple, nearly linear, function of the M-O/T-O ratio, the constant value of *u* in the San Carlos spinels implies that when one of the bond lengths changes as a result of a chemical substitution, the other bond length also changes accordingly in a way that keeps the ratio of bond distances and *u* constant. Both intercrystalline coupled substitution and intracrystalline cation ordering can explain this. In Figure 5, total Al is plotted against total Mg and the inversion parameter for each sample is indicated below its symbol. The main substitution in the Group I San Carlos spinels is Cr for Al at the M site, lengthening M-O, coupled with Fe^{2+} for Mg at the T site, lengthening T-O, in such a way that *u* is kept constant. This sort of coupled substitution is fundamentally different from other coupled substitutions observed in rock-forming minerals such as $Na^{1+} + Si^{4+} = Ca^{2+} + Al^{3+}$ in feldspar. When substitution involves only one site a change in the inversion parameter is observed. Coupled substitutions are limited within the Group

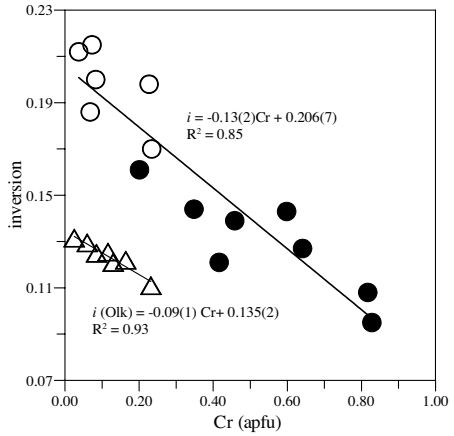

FIGURE 3. Inversion parameters (*i*) vs. Cr. The open triangles represent samples from the Olkhon (Olk) metamorphic complex (Lavina et al. 2003). The solid and open circles represent the samples from Group I and II xenoliths, respectively (this study).

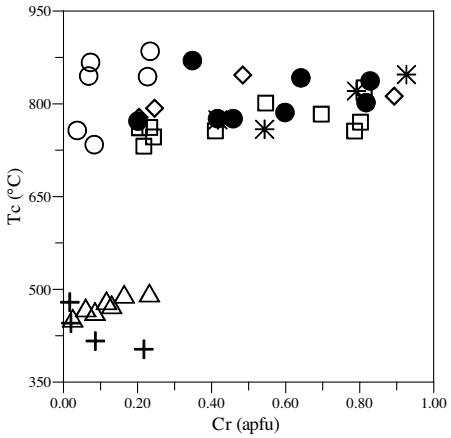

FIGURE 4. Closure temperatures vs. Cr content. The solid circles represent spinels from Group I (this study), open circles from Group II (this study), open squares from Predazzo area (Cararro 2003), open triangles from the Olkhon metamorphic complex (Lavina et al. 2003), open diamond from NE Brazil (Princivalle et al. 1989), asterisks from Ethiopia (Princivalle et al. 1989), and crosses from the Balmuccia peridotite (Basso et al. 1984).

TABLE 5. Oxygen coordinates, inversion parameters, Cr content, and calculated closure temperatures of samples from various environments such as metamorphic, subvolcanic, and volcanic

	Balmuccia	Olkhon	SC (I)	SC (II)	Predazzo	Ethiopia	NE Brazil	Alban Hills
u	0.2635–0.2638	0.2633–0.2635	0.2627–0.2632	0.2627–0.2630	0.2627–0.2630	0.2626–0.2628	0.2624–0.2626	0.2616–0.2624
i	0.06–0.09	0.11–0.13	0.10–0.16	0.17–0.22	0.09–0.18	0.07–0.15	0.09–0.17	0.21–0.28
Cr (apfu)	0.02–0.22	0.02–0.23	0.20–0.83	0.04–0.23	0.21–0.81	0.42–0.93	0.20–0.89	
T (°C)	436 (34)	476 (15)	808 (37)	822 (62)	769 (28)	800 (41)	808 (30)	625–863

Notes: Balmuccia = Basso et al. (1984) and Princivalle et al. (1989); Olkhon = Lavina et al. (2003); SC = Present study; Predazzo = Carraro (2003); Ethiopia and NE Brazil = Princivalle et al. (1989); Alban Hills = Lucchesi et al. (1998).

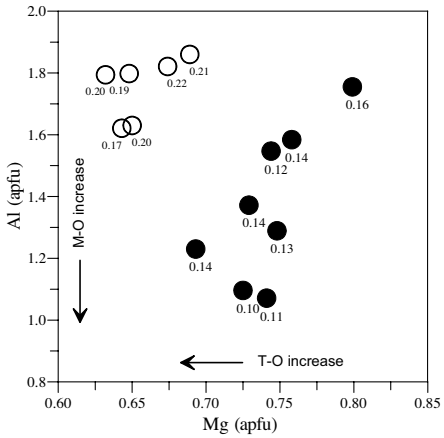

FIGURE 5. Al (apfu) contents in spinels in this study plotted against Mg. The solid circles represent spinels from Group I and open circles from Group II. The inversion parameter is indicated below the symbol for each sample.

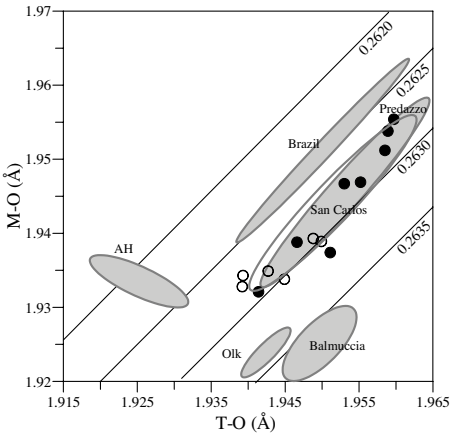

FIGURE 6. Bond distances, M-O vs. T-O, and constant *u* trends. The solid and open circles represent the samples from Group I and II xenoliths, respectively (this study). The sample fields are indicated by shaded ovals: Balmuccia (Basso et al. 1984), Brazil (Princivalle et al. 1989) AH (Lucchesi et al. 1998), Predazzo (Cararro 2003) and Olk (Lavina et al. 2003). Modified after Princivalle et al. (1989).

II suite, but a larger intracrystalline disorder leads to the same oxygen coordinates as found for Group I spinels.

Oxygen coordinates and thermal histories: San Carlos and other localities

Oxygen coordinates (*u*), inversion parameters (*i*), Cr content, and calculated closure temperatures for spinels from various localities are summarized in Table 5. Both types of San Carlos samples show lower inversion parameters than the samples from the Alban Hills volcanic region, which have much simpler chemistry with little Cr, whereas they display similar closure temperatures as some of the Alban Hills samples. Chemistry, structural parameters, and the calculated closure temperatures for Type I spinels from San Carlos are similar to those of the spinels from the Predazzo area (Carraro 2003). It appears that the spinels in both studies experienced similar cooling histories despite different types of host rocks (subvolcanic dikes vs. lava flows).

Bond distances, T-O vs. M-O, are plotted in Figure 6. Lines of constant *u* are superimposed. All the samples shown, except for those from the Alban Hills, lie along lines of constant *u*. In the spinels from Alban Hills, the T-O bond distances are inversely related to M-O, and the oxygen coordinates of the samples from the Alban Hills range from 0.2616 to 0.2624, which suggests those samples experienced slightly different thermal histories within the volcanic region, indicated by their varying closure temperatures. In spite of the extensive chemical variability of San Carlos spinels and the fact that the origins of the two groups of xenoliths are different, the oxygen coordinates remain fixed, suggesting that the oxygen coordinate is a function of thermal history.

ACKNOWLEDGMENTS

We thank T. and E. Goseyun for allowing us to collect samples at their gem mine. Funding for this study was provided by the Tucson Gem and Mineral Society in the form of a scholarship to H. Uchida for her Master's degree. We thank C.T. Prewitt for his assistance and guidance and M. Stimpfl, V.A. Valencia, and two anonymous reviewers for their thoughtful suggestions and comments.

REFERENCES CITED

Andreozzi, G.B. and Lucchesi, S. (2002) Intersite distribution of Fe^{2+} and Mg in the spinel (sensu stricto)-hercynite series by single-crystal X-ray diffraction. American Mineralogist, 87, 1113–1120.

Andreozzi, G.B., Princivalle, F., Skogby, H., and Della Giusta, A. (2000) Cation ordering and structural variations with temperature in $MgAl_2O_4$ spinel: An X-ray single crystal study. American Mineralogist, 85, 1164–1171.

Angel, R.J., Downs, R.T., and Finger, L.W. (2000) High-temperature–high-pressure diffractometry. In R.M. Hazen and R.T. Downs, Eds., High-Temperature and High-Pressure Crystal Chemistry, 41, 559–596. Reviews in Mineralogy and Geochemistry, Mineralogical Society of America, Chantilly, Virginia.

Basso, R., Comin-Chiaramonti, P., Della Giusta, A., and Flora, O. (1984) Crystal chemistry of four Mg-Fe-Al-Cr spinels from the Balmuccia peridotites (Western Italian Alps). Neues Jahrbuch für Mineralogie Abhandlungen, 150, 1–10.

Bernatowicz, T.J. (1981) Noble gases in ultramafic xenoliths from San Carlos, Arizona. Contributions to Mineralogy and Petrology, 76, 84–91.

Bertolo, S. and Nimis, P. (1993) Crystal chemical and structural variations in orthopyroxenes from different petrogenetic environments. European Journal of Mineralogy, 5, 707–719.

Brey, G.P. and Köhler, T.P. (1990) Geothermobarometry in natural four-phase lherzolites, part II: New thermobarometers and practical assessment of existing thermobarometers. Journal of Petrology, 31, 1353–1378.

Bromfield, C.S. and Shride, A.F. (1956) Mineral resources of the San Carlos Indian Reservation Arizona. U.S. Geological Survey Bulletin 1027-N, 613-91.

Burnham, C.W. (1966) Computation of absorption corrections, and the significance of end effect. American Mineralogist, 51, 159–167.

Carbonin, S., Martignago, F., Menegazzo, G., and Dal Negro, A. (2002) X-ray single-crystal study of spinels: in situ heating. Physics and Chemistry of Minerals, 29, 503–514.

Carmichael, I.S.E. (1967) The iron-titanium oxides of salic volcanic rocks and their associated ferromagnesian silicates. Contributions to Mineralogy and Petrology, 14, 36–64.

Carraro, A. (2003) Crystal chemistry of Cr-spinels from a suite of spinel peridotite mantle xenoliths from the Predazzo Area (Dolomites, Nothern Italy). European Journal of Mineralogy, 15, 681–688.

Della Giusta, A., Princivalle, F., and Carbonin, S. (1986) Crystal chemistry of a suite of natural Cr-bearing spinels with 0.15≤Cr≤1.07. Neues Jahrbuch für Mineralogie - Abhandlungen, 155, 319–330.

Della Giusta, A., Carbonin, S., and Ottonello, G. (1996) Temperature-dependent disorder in a natural Mg-Al-Fe^{2+}-Fe^{3+}-spinel. Mineralogical Magazine, 60, 603–616.

Finger, L.W. and Prince, E. (1975) A system of Fortran IV computer programs for crystal structure computations. U.S. National Bureau of Standards, Technical Note 854, 128 pp.

Frey, F.A. and Green, D.H. (1974) The mineralogy, geochemistry and origin of lherzolite inclusions in Victorian basanites. Geochimica et Cosmochimica Acta, 38, 1023–1059.

Frey, F.A. and Prinz, M. (1978) Ultramafic inclusions from San Carlos, Arizona: Petrologic and geochemical data bearing on their petrogenesis. Earth and Planetary Science Letters, 38, 129–176.

Galer, S.J.G. and O'Nions, R.K. (1989) Chemical and isotopic studies of ultramafic inclusions from the San Carlos volcanic field, Arizona: A bearing on their petrogenesis. Journal of Petrology, 30, 1033–1064.

Ganguly, J. (1982) Mg-Fe order-disorder of ferromagnesian silicates. II. Thermodynamics, kinetics, and geological applications. In S.K. Saxena, Ed., Advances in Physical Geochemistry, 2, 58–99. Springer, Berlin Heidelberg New York.

Hamilton, W.C. (1974) Normal probability plots. International Tables for X-ray Crystallography. The Kynoch Press. Birmingham, England.

Hazen, R.M. and Navrotsky, A. (1996) Effects of pressure on order-disorder reactions. American Mineralogist, 81, 1021–1035.

Hill, R.J., Craig, J.R., and Gibbs, G.V. (1979) Systematics of the spinel structure type. Physics and Chemistry of Minerals, 4, 317–339.

Ibers, J.A. and Hamilton, W.C., Eds. (1974) International Tables for X-ray Crystallography, vol. IV, 366 p. Kynoch, Birmingham, U.K.

King, H.E. and Finger, L.W. (1979) Diffracted beam crystal centering and its application to high-pressure crystallography. Journal of Applied Crystallography, 12, 374–378.

Köhler, T.P. and Brey, G.P. (1990) Calcium exchange between olivine and clinopyroxene calibrated as a geothermobarometer for natural peridotites from 2 to 60 kb with applications. Geochimica et Cosmochimica Acta, 54, 2375–2388.

Lavina, B., Salviulo, G., and Della Giusta, A. (2002) Cation distribution and structure modeling of spinel solid solutions. Physics and Chemistry of Minerals, 29, 10–18.

Lavina, B., Koneva, A., and Della Giusta, A. (2003) Cation distribution and cooling rates of Cr-substituted Mg-Al spinel from the Olkhon metamorphic complex, Russia. European Journal of Mineralogy, 15, 435–441.

Levy, D., Pavese, A., and Hanfland, M. (2003) Synthetic $MgAl_2O_4$ (spinel) at high-pressure conditions (0.0001-30 GPa): A synchrotron X-ray powder diffraction study. American Mineralogist, 88, 93–98

Lucchesi, S. and Della Giusta, A. (1997) Crystal chemistry of a highly disordered Mg-Al natural spinel. Mineralogy and Petrolgy, 59, 91–99.

Lucchesi, S., Amoriello, M., and Della Giusta, A. (1998) Crystal chemistry of spinels from xenoliths of the Alban Hills volcanic region. European Journal of Mineralogy, 10, 473–482.

Marlowe, J.I. (1961) Late Cenozoic geology of the lower Safford basin on the San Carlos Indian Reservation, Arizona. Ph.D. Thesis, University of Arizona.

Nimis, P. (1995) A clinopyroxene geobarometer for basaltic systems based on crystal-structure modeling. Contributions to Mineralogy and Petrology, 121, 115–125.

——— (1999) Clinopyroxene geobarometry of magmatic rocks. Part 2. Structural geobarometers for basic to acid, tholeiitic and mildly alkaline magmatic systems. Contributions to Mineralogy and Petrology, 135, 62–74.

Nimis, P. and Ulmer, P. (1998) Clinopyroxene geobarometry of magmatic rocks. Part 1: An expanded structural geobarometer for anhydrous and hydrous, basic and ultrabasic systems. Contributions to Mineralogy and Petrology, 133, 122–135.

O'Neill, H.St.C (1994) Temperature dependence of the cation distribution in $CoAl_2O_4$ spinel. European Journal of Mineralogy, 6, 603–609.

O'Neill, H.St.C. and Navrotsky, A. (1983) Simple spinels: crystallographic parameters, cation radii, lattice energies, and cation distribution. American Mineralogist, 68, 181–194.

O'Neill, H.St.C., Redfern, S.A.T., Kesson, S., and Short, S. (2003) An in-situ neutron diffraction study of cation disordering in synthetic qandilite Mg_2TiO_4 at high temperatures. American Mineralogist, 88, 860–865.

Pavese, A., Artioli, G., Russo, U., and Hoser, A. (1999) Cation partitioning versus temperature in $(Mg_{0.70}Fe_{0.23})Al_{1.97}O_4$ synthetic spinel by in situ neutron powder diffraction. Physics and Chemistry of Minerals, 26, 242–250.

Peterson, R.C., Lager, G.A., and Hitterman, R.L. (1991) A time-of-flight neutron powder diffraction study of $MgAl_2O_4$ at temperatures up to 1273 K. American Mineralogist, 76, 1455–1458.

Pouchou, J.L. and Pichoir, F. (1991) Quantitative analysis of homogeneous or stratified microvolumes applying the model "PAP". In K.F.J. Heinrich and D.E. Newbury, Eds., Electron Probe Quantitation, pp. 31–75. Plenum Press, New York.

Princivalle, F., Della Giusta, A., and Carbonin, S. (1989) Comparative crystal chemistry of spinels from some suites of ultramafic rocks. Mineralogy and Petrology, 40, 117–126.

Princivalle, F., Della Giusta, A., De Min, A., and Piccirillo, E.M. (1999) Crystal chemistry and significance of cation ordering in Mg-Al rich spinels from high-grade hornfels (Predazzo-Monzoni, NE Italy). Mineralogical Magazine, 63, 257–262.

Redfern, S.A.T., Harrison, R.J., O'Neill, H.St.C., and Wood, D.R.R. (1999) Thermodynamics and kinetics of cation ordering in $MgAl_2O_4$ spinel up to 1660 °C from in situ neutron diffraction. American Mineralogist, 84, 299–310.

Schmocker, U. and Waldner, F. (1976) Inversion parameter with respect to space group of $MgAl_2O_4$ spinels. Journal of Physics C-Solid State Physics, 9, L235–L237.

Stimpfl, M. (2003) Experimental studies of Fe^{2+}–Mg order–disorder in orthopyroxene: equilibrium, kinetics, and applications. Ph.D. thesis. University of Arizona, Tucson.

Stimpfl, M., Ganguly, J., and Molin, G. (1999) Fe^{2+}-Mg order-disorder in orthopyroxene: equilibrium fractionation between the octahedral sites and thermodynamic analysis. Contributions to Mineralogy and Petrology, 136, 297–309.

Thompson, R.M. and Downs, R.T. (2001) Quantifying distortion from ideal closest-packing in a crystal structure with analysis and application. Acta Crystallographica, B57, 119–127.

Wilshire, H.G. and Shervais, J.W. (1975) Al-augite and Cr-diopside ultramafic xenoliths in basaltic rocks from western United States. Physics and Chemistry of the Earth, 9, 257–272.

Wohletz, K.H. (1978) The eruptive mechanism of the Peridot Mesa vent, San Carlos, Arizona. Geological Society of America. Cordilleran Section Special Paper No 2, 167–176.

Zartman, R.E. and Tera, F. (1973) Lead concentration and isotopic composition in five peridotite inclusions of probable mantle origin. Earth and Planetary Science Letters, 20, 54–66.

Zindler, A. and Jagoutz, E. (1980) Isotope and trace element systematics in mantle-derived peridotite nodules from San Carlos. EOS, 61, 374.

——— (1988) Mantle cryptology. Geochimica et Cosmochimica Acta, 52, 319–333.

MANUSCRIPT RECEIVED AUGUST 24, 2004
MANUSCRIPT ACCEPTED FEBRUARY 22, 2005
MANUSCRIPT HANDLED BY LEE GROAT